NANOPARTICLE-COATED POLYMERIC MICROBUBBLES FOR REVASCULARIZATION

BY

JINRONG CHEN

THESIS

Submitted in partial fulfillment of the requirements
for the degree of Master of Science in Chemical Engineering
in the Graduate College of the
University of Illinois at Urbana-Champaign, 2015

Urbana, Illinois

Adviser:

Associate Professor Hyunjoon Kong

ABSTRACT

Nano-sized materials have been widely used in many products, such as painting materials, cosmetics, and drug cargos. Especially in biological applications, nanoparticles work as drug delivery carriers in recent decades due to their features on size and transport properties compared to drug molecules alone. Modification of nanoparticle surface, structure, and its fabrication methods has been done by researchers to improve the loading efficiency and targeting performance. However, the retention of nanoparticles on the targeted tissue is still a big challenge. After injection, drug loaded nanoparticles are rapidly washed away in the area of drug delivery due to high local velocity, which limits the drug release on the desired site. In this study, we hypothesized that the nanoparticles are able to coat over the microbubble surface spontaneously through van der Waals attraction without any chemical or electrical modification on the particle surface, where the microbubble were self-assembled by the amphiphilic polymer. Microbubbles are commonly used as ultrasound contrast agents, and the limited life time of microbubbles is the major challenge for microbubble applications. The coating of the nanoparticles enhanced the microbubbles' stability, and at the same time, the microbubbles helped to reduce the movement of the nanoparticles. Moreover, the immobilization of nanoparticles improved the performance of nanoparticle retention and the effect of drug deliver. The results provide a new strategy of the co-existence of micro- and nano-scaled particles without the additional surface tailoring and a new research direction of the improved drug retention on targeted tissue.

TABLE OF CONTENTS

Chapter 1

INTRODUCTION

1.1 Background and Motivation

In recent decades, tons of studies on micro- and nano-sized materials have been done, and nanoparticles have been involved within daily life in many aspects, such as painting material, cosmetics, and food.[1-3] Among these developments, the use of nanoparticles in biological application has drawn a lot of attention. As a biocompatible material, the big potential market of nanoparticles in biological applications has expanded fleetly.[4-6] Nanoparticles are capable of loading drug molecules of interests and also sustainably releasing the molecules. They have been extensively studied to improve quality of molecular therapies because nanoparticles' uniquely size enables minimally invasive delivery via simple intravenous or intramuscular injection. It is well agreed that the successful use of nanoparticles in drug delivery greatly relies on a capability to retain the particles in target tissue over a desired treatment time period.[7-11] However, nanoparticles are readily displaced from the implanted site, particularly when the area is subject to external mechanical force. The resulting increase of drift velocity becomes more significant with smaller particles. Therefore, there is a great need to improve a nanoparticle retention level in a target tissue defect or pathologic tissue.[12-14]

To resolve such challenges, certain efforts were made to reduce mobility of nanoparticles following injection. For example, nanoparticles were mixed with a pre-gel solution to be entrapped in the gel, where the gel can prevent displacement of nanoparticles. To further improve retention of nanoparticles in a gel, nanoparticle surface

was modified to electrostatically associate with gel-forming polymers. However, this approach was often fraught by reduced molecular release rate, because the gel matrix acted as a physical barrier that decreased diffusivity of drug molecules following the release from nanoparticles. Alternatively, surface potential of nanoparticles was engineered to induce electrostatic attraction between them, so the nanoparticles are self-assembled to form a colloidal gel following injection.[15,16] However, surface potential of nanoparticles may negatively influence drug release rate via uncontrolled electrostatic interaction. Therefore, there are grand interests in reducing nanoparticle mobility without loading them in a gel matrix or altering surface potential of nanoparticles.

To this end, we hypothesized that van der Waals force-induced loading of nanoparticles onto surface of sacrificial, micro-sized polymeric bubbles with tissue epithelium would allow us to significantly elevate nanoparticle retention level at injected sites, even without altering surface potential of nanoparticles.

1.2 Research Plan

In this study, we examined the hypothesis by using microbubbles with an average diameter of about 50 μm, formed from self-assembly of alkylated polyaspartamide as a model of sacrificial microbubbles. The poly(lactic-co-glycolic acid) (PLGA) nanoparticles with an average diameter of about 100 nm was used as a model of drug-loaded nanoparticles. Due to the difference in the diameters of microbubbles and nanoparticles by two orders of magnitude, van der Waals attraction between microbubble and nanoparticle becomes larger than the attraction between PLGA nanoparticles. The role of microbubbles in improving retention level of PLGA nanoparticle was evaluated

by implanting the fluorescent nanoparticle-coated microbubbles onto chicken chorioallantoic membranes (CAMs) and quantifying the fluorescent intensity. The effect of nanoparticle retention on drug efficacy was further evaluated by using PLGA nanoparticles laden with angiopoetin-1 on CAMs and examining the degree of neovascularization.

Chapter 2

MATERIALS AND METHODS

2.1 Synthesis and characterization of PHEA-g-C_{18}

Briefly, poly(succinimide) (PSI, Mw 19,000 g/mol, PDI 1.5) was the starting chemical, synthesized through the acid-catalyzed polycondensation process of L-aspartic acid (Sigma-Aldrich) described previously.[17] The L-aspartic acid was dissolved in dried sulfolane with existence of 85% phosphoric acid as the catalyst to generate PSI with molecular weight of 19,000 g/mol. The reaction happened at 170 °C for 7 hours, refluxed under dry nitrogen atmosphere with Dean-Stark trap setup (Figure 2.1). The color change was observed while the reaction was going on. After the reaction was done, the precipitation was filtered out, and washed with methanol and deionized water in sequence till it was neutral. Then dialyze (Fisher Scientific, MWCO 3,500) the product against deionized water for two days and freeze dry (Labconco, FreeZone 6) to obtain dry powder.

By aminolysis, PSI was functionalized with octadecylamine (ODA) (Sigma-Aldrich) and ethanolamine (Sigma-Aldrich) sequentially into poly(2-hydroxyethyl aspartamide) grafted with octadecyl chains (PHEA-g-C_{18}).[18] PSI, dissolved in dimethylformamide (DMF) at concentration of 1.5 mmol PSI per 5 mL DMF, was reacted with the calculated amount of ODA at 70 °C for 24 hours with continuous stirring. After the mixture was cooled down to the room temperature, the calculated volume of ethanolamine was added dropwise and further reacted for 6 hours. The final product was collected and purified via dialysis (Fisher Scientific, MWCO 3,500) against

deionized water for 2 days followed by freeze-drying (Labconco, FreeZone 6) to obtain the dry powder.

The structure of PHEA-g-C_{18} was characterized by ^{1}H NMR spectra, from which the degree of substitution of octadecyl chains (DS_{C18}) on the PHEA backbone was calculated by using [Eq. (1)]:

$$DS_{C18} = \frac{Integration\ of\ spectra\ from\ 0.80\ to\ 0.86\ /3}{Integration\ of\ spectra\ from\ 4.36\ to\ 4.70}. \qquad \text{Eq. (1)}$$

where the integration of spectra from 0.80 ppm to 0.86 ppm represents the methyl group on octadecyl chain containing three protons; the integration of spectra from 4.36 ppm to 4.7 ppm represents the proton on the polymer backbone with one per polymer unit.

2.2 Formation of microbubbles

Pre-microbubble solution was prepared by dissolving PHEA-g-C_{18} in deionized water at concentrations of 0.1% w/w, 0.5% w/w and 1% w/w in 1.5 mL Eppendorf tube with necessary Vortex touch mixing (Scientific Industries) and bath sonication (Fisher Scientific, FS60). To form bubbles, the probe sonicator (Fischer Scientific, Sonic Dismembrator Model 100) was applied, where the tip of the sonicator probe was placed about 2 mm under the liquid surface (Figure 2.2). Under the average output power of 6 watts for 30 seconds, a foam layer of microbubbles was generated. Followed by the fabrication of non-coating microbubbles described previously, the microbubbles coated with functionalized PLGA nanoparticles were prepared by carefully replacing the deionized water media with prepared 0.5% w/w PLGA nanoparticle solution.

2.3 Characterization of microbubbles

The diameters of microbubbles at different concentrations and different time points were measured through optical microscope images (Leica, DMIL) by using ImageJ. The microbubble sample was fixed on the surface of agar gel to immobilize the microbubbles for imaging. The agar gel was prepared by dissolving agar powder (Sigma) in deionized water at 10% w/w and heating the suspension at 85 ℃ till it was clear. Then pour the pre-gel solution into a Petri dish and gently transfer microbubbles in the center of the gel surface. The sample was ready to use till the gel was completed congealed.

To analyze the stability of microbubbles, the microbubble solution was kept in 1.5 mL Eppendorf tube and incubated at 37 ℃ overtime. A certain amount of microbubble was taken from each sample at the time point of 0 hour, 1 hour, and 3 hours, and the diameters were measured from optical microscopy images (Leica, DMIL) with Image J. The PLGA nanoparticle coating on the microbubble surface was observed with confocal microscopy images (Zeiss, LSM700), while PLGA nanoparticles were labeled with fluorescein isothiocyanate (FITC) (Sigma-Aldrich).

2.4 Preparation of PLGA nanoparticles

Nano-sized PLGA particles were generated through nanoprecipitation process, where the solution of PLGA (Direct) in acetone was added dropwise into deionized water with continuous stirring. After the precipitation, the organic solvent was evaporated under fume hood over night or by rotary evaporator, and the PLGA nanoparticles were dried via lyophilization (Labconco, FreeZone 6). For fluorescent PLGA nanoparticles,

FITC was added at the step of dissolving PLGA in acetone. For angiopoietin-1 loaded PLGA nanoparticles, a certain amount of angiopoietin-1 was dissolved and diluted in 1x phosphate buffered saline (1x PBS). Instead of dropping solution of PLGA in acetone into deionized water, the polymer solution was added into 1x PBS solution of angiopoietin-1 dropwise.

2.5 Retention test of nanoparticles

Chick chorioallantoic membrane (CAM) assay was used to analyze the retention behavior of the fluorescent PLGA nanoparticles at the conditions with and without microbubbles. The eggs were one week old, fertilized chicken embryos from the farm. A window with the diameter about 1 cm on the egg shell was opened one day before the sample implantation. Samples were placed onto the CAMs and incubated at 37 ℃. During the incubation, the window on the egg shell was always covered with a piece of transparent tape. After time points of 1 hour, 1 day, and 7 days, CAMs of three eggs for each condition were excised at the implantation area after adding 2 mL 3.7% v/v formaldehyde (Sigma-Aldrich) and storing at 4 °C for an hour. Then the CAMs were cut out from the eggs and kept in Petri dishes with sufficient amount of 3.7% v/v formaldehyde (Figure 2.3). The distribution of fluorescent PLGA nanoparticles on CAMs were observed with confocal microscopy images (Zeiss, LSM700), and the total fluorescent areas and the nanoparticle aggregation areas were quantified by MATLAB code developed by the author.

2.6 Angiogenesis with angiopoietin-1 loaded particles

Angiopoietin-1 loaded PLGA nanoparticles with or without microbubbles were implanted onto the CAMs followed by the CAM assay process described in session 2.5. Instead of excising the eggs at different time points, all the eggs were sacrificed after 7 days for angiogenesis study. Here, 1x PBS was used as a control group without any elevating on vascularization. The excised CAMs on day 7 were embedded in paraffin, sectioned, and stained with an antibody to α-smooth muscle actin (α-SMA) for histological study. The images of CAM cross sessions were taken with the optical microscope (Leica, DMIL), and the number of the blood vessels with cross sectional area less than 500 μm^2 was quantified by Image J.

2.7 Figures

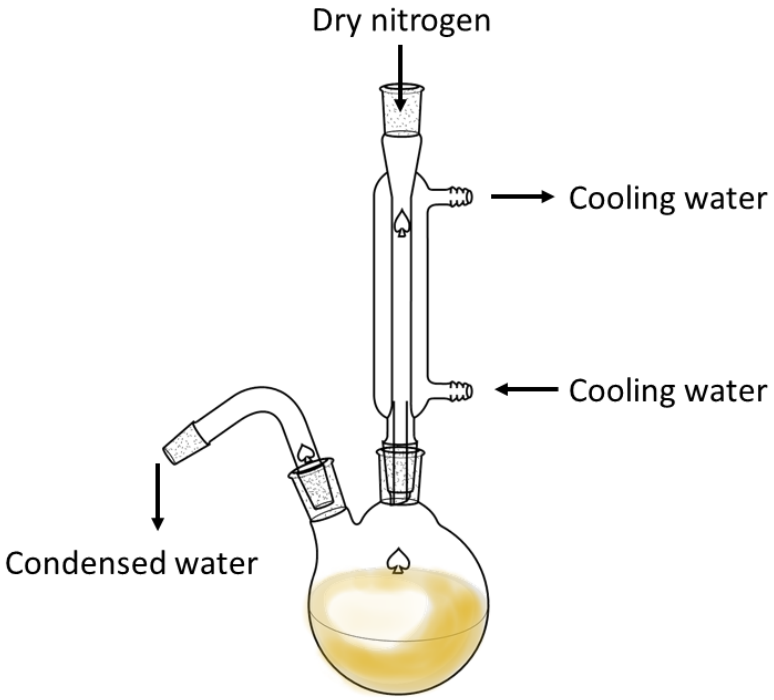

Figure 2.1. The experiment setup of the acid-catalyzed polycondensation of L-aspartic acid to form PSI with Dean-Stark trap.

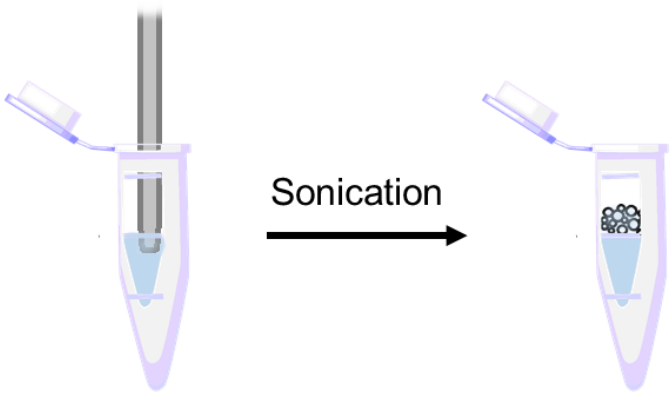

Figure 2.2. The experiment setup of microbubble generation by probe sonication.

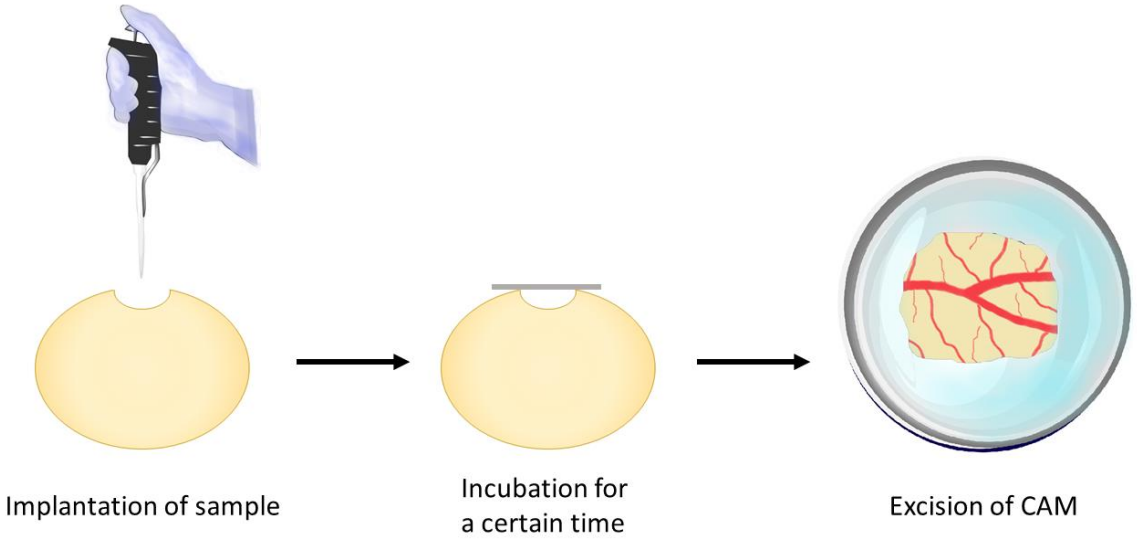

Figure 2.3. The scheme of CAM experiment for retention and angiogenesis evaluation.

Chapter 3

RESULTS AND DISCUSSION

3.1 Preparation and characterization of polymeric microbubbles

Microbubbles were formed via self-assembly of amphiphilic polymer – poly(2-hydroxyethyl aspartamide) grafted with octadecyl chains, termed as PHEA-g-C_{18}. In the first step, polycondensation of $_L$-aspartic acid with acid catalyst led to polysuccinimide (PSI). Secondly, PSI was substituted with octadecylamine and ethanolamine to form PHEA-g-C_{18} by aminolysis reactions, where the hydroxyl groups acted as the hydrophilic component and the alkyl chains acted as the hydrophobic component (Figure 3.1a).[17,18] At a molar ratio between octadecylamine and succinimidyl units of PSI at 15%, the final degree of substitution for octadecyl chains (DS_{C18}) was 12.2 mol% as quantified with peaks from 0.80 to 0.86 ppm and peaks from 4.36 to 4.70 ppm in from ^{1}H NMR spectra by using Eq(1) (Figure 3.1b). Note that peaks from 0.80 to 0.86 ppm represent protons of methyl groups at the end of the C_{18} chains containing three protons and those from 4.36 to 4.70 ppm do PHEA backbones containing one proton per PSI unit.

The resulting, amphiphilic PHEA-g-C_{18} was able to self-assemble into microbubbles by sonication applied at the interface of air and polymer solution (Figure 3.2). Particularly, microbubbles were assembled with polymer solutions at three different concentrations of the polymer solution to control size and stability (Figure 3.3a). Increasing concentration of the polymer solution from 0.1% to 0.5% w/w decreased the initial average diameter of microbubbles. The sizes of microbubbles were quantified with optical images, and as the result, as the concentration increases, the average diameter of

the microbubbles decreased from 194 ± 103 µm to 49 µm ± 36 µm. Further increasing the polymer concentration to 1% w/w made the minimal changes of the initial diameter of microbubbles; however, it contributed to improving the stability of bubbles incubated at 37 ℃. Over 3 hours, the microbubbles prepared with 1% w/w polymer solution undertook a two-fold smaller increase of the diameter compared to the ones with 0.5% w/w polymer solution (Figure 3.3b).

It suggested that sonication applies enough energy to direct hydrophobic association of octadecyl chains of PHEA in oil phase with air molecules. Then, the polymers surround air molecules to reduce the thermodynamic free energy. Finally, hydroxyl groups of PHEA-g-C_{18} likely facilitate dispersion of microbubbles in aqueous media. Therefore, similar to a surfactant, increasing concentration of PHEA-g-C_{18} from 0.1% to 0.5% w/w should lead to an increase of the curvature of microbubbles. The minimal change of the microbubble size with an increase of polymer concentration from 0.5% to 1% w/w indicates that polymer association with air molecules is saturated at 0.5% w/w. The significantly enhanced microbubble stability marked by a smaller size increase implicates that excess PHEA-g-C_{18} in the media prevents association between microbubbles and subsequent fusion.

3.2 Modification of microbubbles coated with PLGA nanoparticles

Monodisperse PLGA nanoparticles with an average diameter of 100 nm were prepared via nanoprecipitation. Mixing aqueous suspension of PLGA nanoparticles with freshly made microbubbles resulted in microbubbles spontaneously covered by PLGA

nanoparticles (Figure 3.4a). According to fluorescence imaging of PLGA nanoparticles labeled with fluorescein isothiocyanate (FITC) in free suspension and co-existence with microbubbles, nanoparticles were clearly localized on surface of microbubbles (Figure 3.4b and 3.4c). Even after the exposure to shear flow to simulate injection process, the nanoparticles were stably bound to the microbubble.

It is suggested that the association between microbubbles and nanoparticles are driven by van der Waals attraction forces, due to significantly different size by one order of magnitude [Eq. (2)]:

$$V_A = -\frac{A}{6D}\frac{R_1 R_2}{R_1 + R_2} \qquad \text{Eq. (2)}$$

where R_1 and R_2 are the radii of microbubbles and nanoparticles respectively; A is the Hamaker constant with unit of Joule; V_A is van der Waal potential; and D is the distance between two particles.[19] The Hamaker constants of PHEA-g-C_{18} and PLGA were considered 6.5×10^{-20} J.[20] The estimated attractive energy potential between PLGA nanoparticle and microbubble is about twice of that between two PLGA nanoparticles, and the size of microbubbles did not really affect the van der Waal potential (Table 3.1).

More interestingly, the mirocbubbles coated with PLGA nanoparticles remained more stable than plain microbubbles in a physiologically relevant condition. At 37 ℃, the microbubbles prepared with 1% w/w PHEA-g-C_{18} solution undertook a three-fold smaller increase of the diameter than bare microbubbles (Figure 3.5a). With the nanoparticle coating, all most the whole population of microbubbles was within the diameter smaller than 50 μm at the beginning; even after 3 hours, there were still around 70% of microbubbles in the range within 50 μm. In contrast, without nanoparticle coating, only

about 70% of microbubbles appeared with less than 50 μm in diameter; after 3 hours, the majority of bare microbubbles was in the range of 100 to 250 μm (Figure 3.5b).

3.3 In vivo evaluation of PLGA nanoparticle retention

The PLGA nanoparticles and those associated with microbubbles, both of which were labeled with fluorescent molecules FITC, were placed on chicken chorioallantoic membrane (CAM), in order to evaluate retention level of PLGA nanoparticles with fluorescence. According to fluorescence imaging of the CAMs captured after implantation, both two conditions displayed minimal change of fluorescence yield after one hour of implantation (Figure 3.6a). Given that fluorescent molecules were conjugated with PLGA nanoparticles, this result implicates that nanoparticle displacement was minimal during first one hour (Figure 3.6b).

However, between Day 1 and Day 7, the total fluorescence from PLGA nanoparticles implanted without being associated with microbubbles rapidly decreased (Figure 3.6c). According to the quantification with fluorescence yield, approximately 90% of PLGA nanoparticles were displaced from the implanted site without microbubbles. In contrast, the nanoparticles associated microbubbles exhibited no significant decrease of fluorescence over 7 days. Overall, almost all PLGA nanoparticles were remained in the implanted site due to microbubbles.

Given that PHEA-g-C_{18} microbubbles are collapsed within a few hours of implantation, but the majority of polymers remain at the implantation site. We suggest that PHEA-g-C_{18} from the collapsed microbubbles hydrophobically associate with

epithelium of CAMs to reduce the PLGA nanoparticle movement; in contrast, without microbubbles and PHEA-g-C_{18}, PLGA nanoparticles are quickly replaced and aggregate in small groups on CAMs (Figure 3.7a and 3.7b). Therefore, it is likely that the PHEA-g-C_{18} could reduce the number of PLGA nanoparticles displaced by mechanical deformation of CAM caused by an embryo's heart contraction. Additionally, the minimal difference of the number of PLGA nanoparticles between two conditions at Hour 1 implicates that free PLGA nanoparticles could initially associate with CAMs. However, the adhesion strength of PLGA nanoparticles to CAMs is likely smaller than that to PHEA-g-C_{18} microbubbles, due to the absence of hydrophobic alkyl chains on its surface as well as higher mobility. In this regard, the conjugation of alkyl chains to PLGA nanoparticle surface may reduce nanoparticle displacement even without the appearance of PHEA microbubbles. However, the underlying chemistry may negatively impact encapsulation efficiency and bioactivity of encapsulated drug molecules. In this regard, it would be advantageous to separately use PLGA nanoparticles as a drug carrier and PHEA-g-C_{18} microbubbles as a tissue glue.

3.4 In vivo evaluation of vascularization induced by Angiopoietin-1 loaded PLGA nanoparticles

To demonstrate the importance of the retention of drug-releasing PLGA nanoparticles in therapies, PLGA nanoparticles loaded with Angiopoietin-1. Angiopoietin-1 is known to stimulate angiogenesis by activating Tol-like receptors of endothelial progenitor and precursor cells.[21] The Angiopoietin-1 loaded in the PLGA

nanoparticles are sustainably released within first five days, so they can stimulate host blood vessel-forming cells. The Angiopoietin-1 encapsulating PLGA nanoparticles further associated with PHEA-g-C_{18} microbubbles were implanted on the CAM, as well as control conditions including PBS buffer and mirobubble-free Angiopoietin-1 releasing PLGA nanoparticles.

According to cross-sectional histological images of the CAM stained for alpha-smooth muscle actin layer on mature blood vessels, the membranes implanted with Angiopoietin-1-releasing PLGA nanoparticles presented about five-fold larger number of mature blood vessels with cross-sectional area between 30 and 400 μm^2 those injected with PBS (Figure 3.8). In contrast, CAM implanted with PLGA nanoparticles immobilized on the sacrificial PHEA-g-C_{18} microbubbles presented the more than six-fold increase of the number of mature blood vessels. In addition, the microbuubles contributed to improving neovascularization efficacy of Angiopoietin-1 releasing PLGA nanoparticles by three times (Figure 3.9).

We interpret that such enhanced neovascularization using PLGA nanoparticles immobilized on microbuubles is well correlated to the improved retention of PLGA nanoparticles at an implantation site, as displayed in Figure 3. The Angiopoietin-1-releasing, bare PLGA nanoparticles do not chemically or physically interact with epithelium that constitute CAM. Therefore, the nanoparticles are likely displaced from the implanted site, thus reducing bioavailability of Angiopoietin-1. In contrast, PLGA nanoparticles remained at the implantation site due to association with PHEA-g-C_{18} microbubbles should be able to increase concentration of Angiopoietin-1 and activating cellular signaling involved with endothelial sprouts and smooth muscle cell recruitment.

It is well agreed that density and quality of newly-forming blood vessels are significantly dependent on the duration of proangiogenic growth factors. We believe that such nanoparticle delivery strategy using microbubbles would be used for a variety of growth factors known to stimulate tissue regeneration. There material systems will be ultimately contribute to improving quality of various wounds and tissue defects with reduced dosage of growth factors.

3.5 Figures and Tables

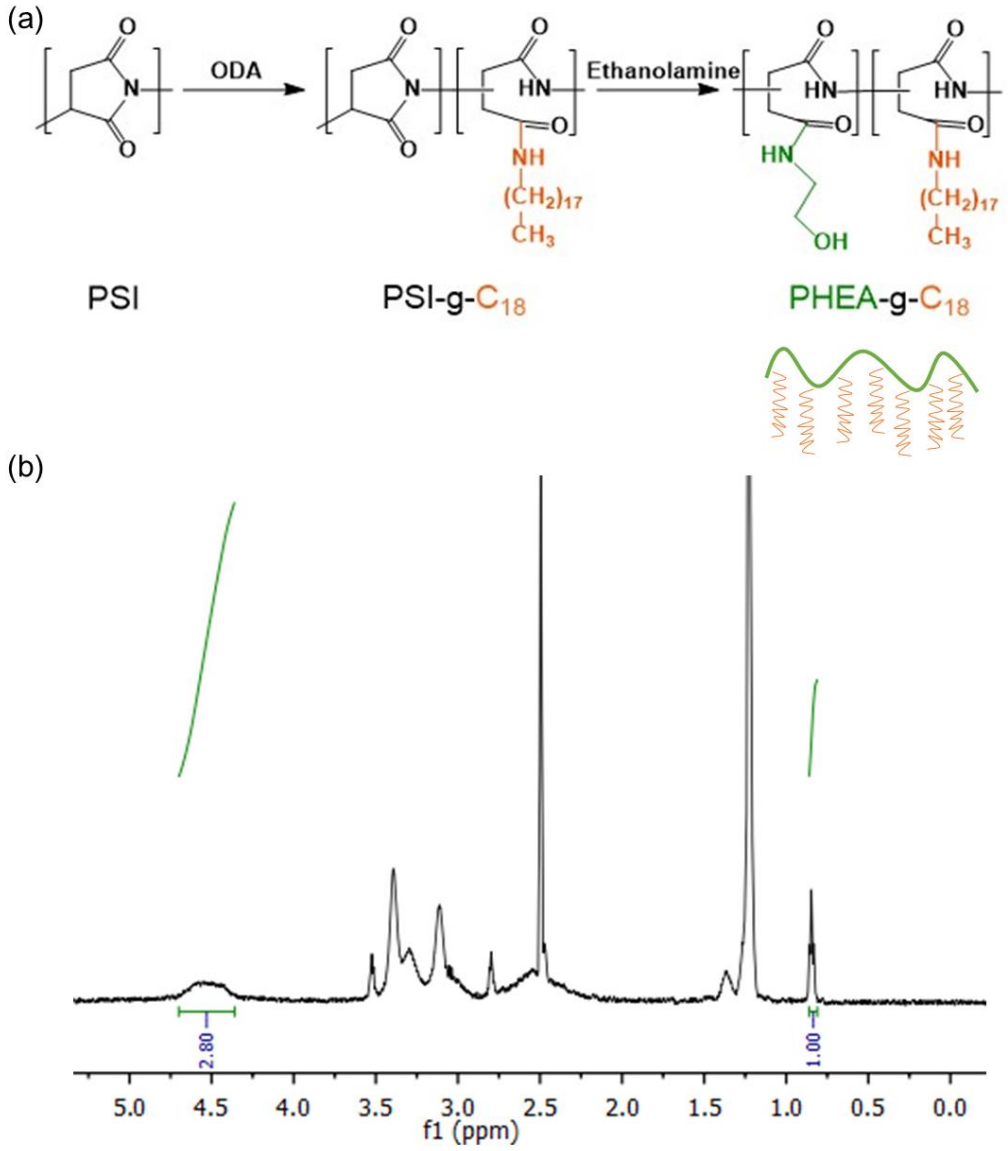

Figure 3.1. Synthesis of PHEA-g-C_{18} microbubbles. (a) The reaction scheme of PHEA (green) functionalized with octadecyl chains (C_{18}) (orange). (b) ^{1}H NMR spectra of PHEA-g-C_{18} with integration.

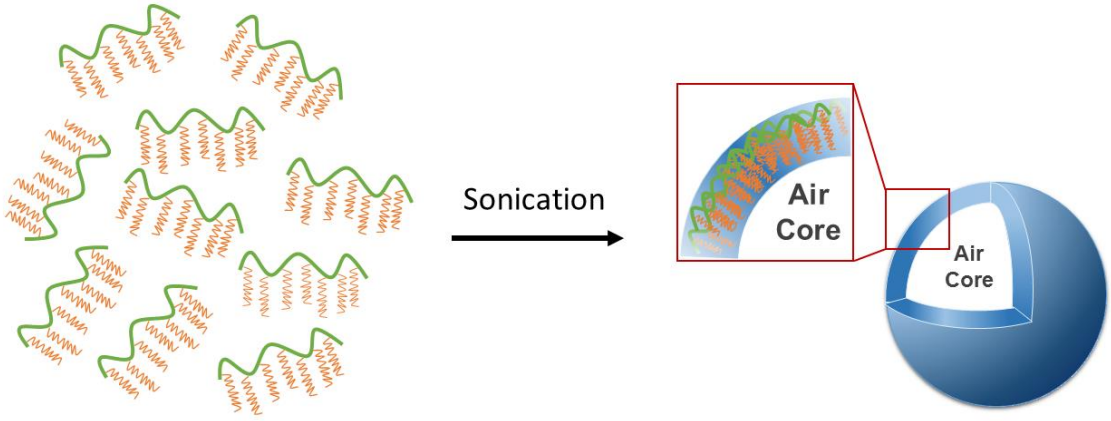

Figure 3.2. Scheme of microbubble formation by probe sonication at molecular level: After sonication at the interface of air and polymer aqueous solution, the alkyl chains were towards the air core regarded as an oil phase, and the hydroxyl groups on the polymer backbone stabilized the microbubbles in aqueous phase.

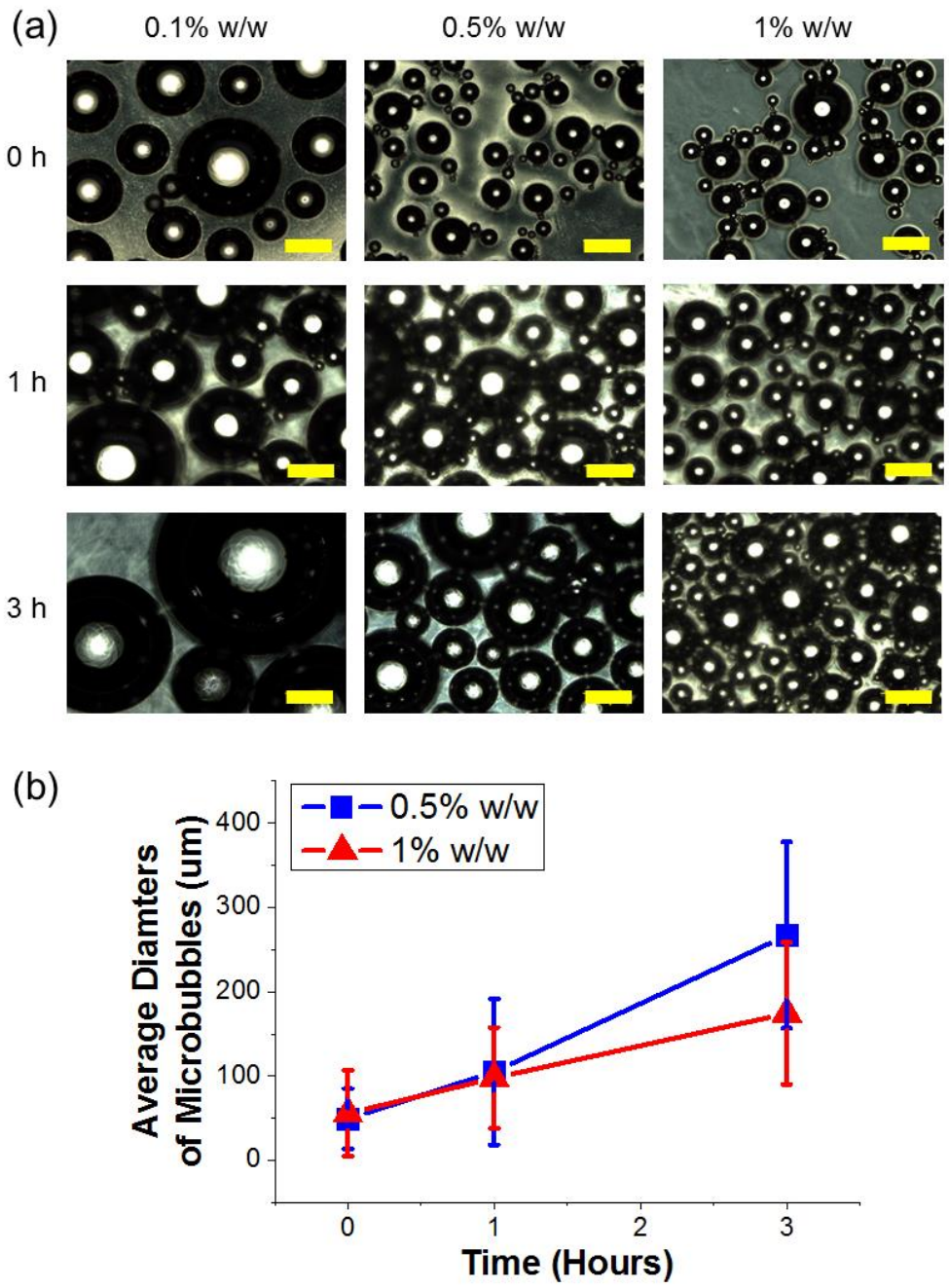

Figure 3.3. Characterization of PHEA-g-C_{18} microbubbles. (a) Optical microscopy images of microbubbles prepared with solution of three different PHEA-g-C_{18} concentrations. The bubbles were captured at different time points while incubating them in deionized water. Scale bar represents 200 μm. (b) The growth trend of microbubbles at conditions of 0.5% and 1% w/w over 3 hours. With 0.5% w/w solution, 512, 231, and 63 microbubbles were measured respectively at 0 hour, 1 hour, and 3 hours; with 1% w/w solution, 514, 349, and 126 microbubbles were measured respectively at 0 hour, 1 hour, and 3 hours.

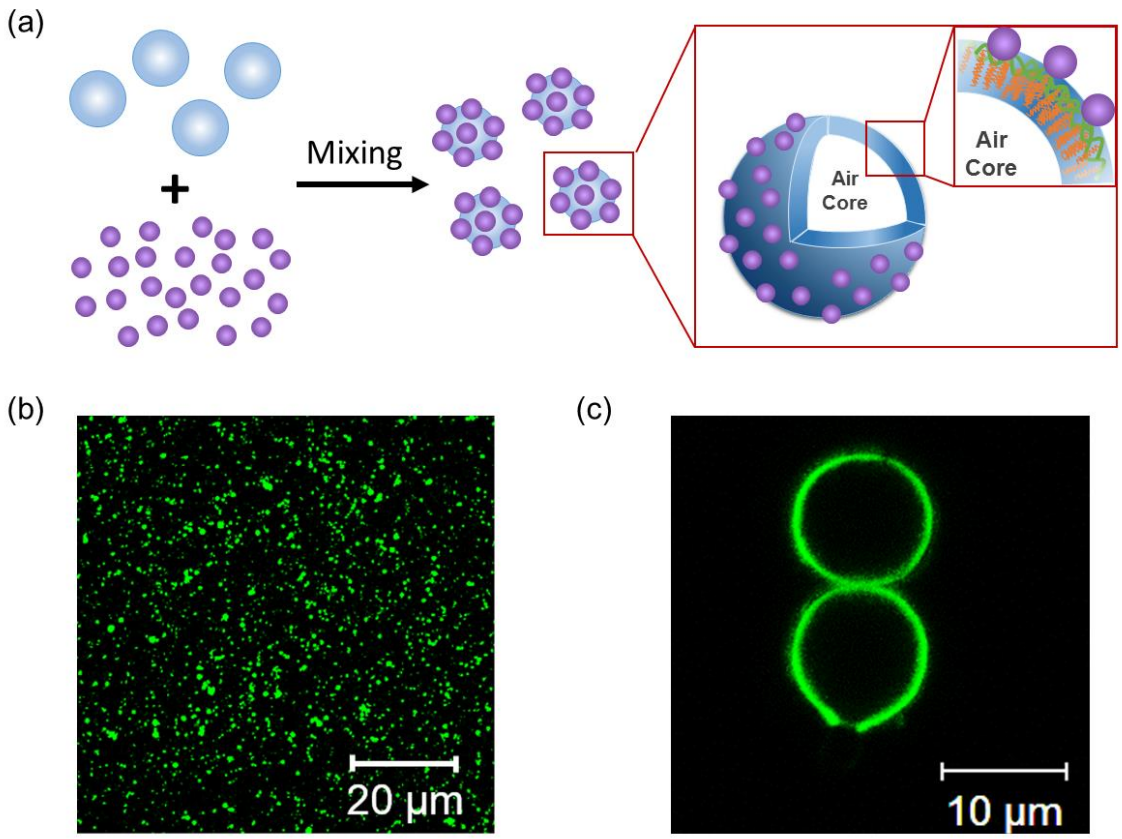

Figure 3.4. Modification of microbubbles coated with PLGA nanoparticles. (a) The schematic structure of microbubbles (the blue sphere) coated with PLGA nanoparticles (the purple spheres). (b) The confocal microscopy image of pure FITC-labeled PLGA nanoparticles. (c) The confocal microscopy image of microbubbles coated with FITC-labeled PLGA nanoparticle.

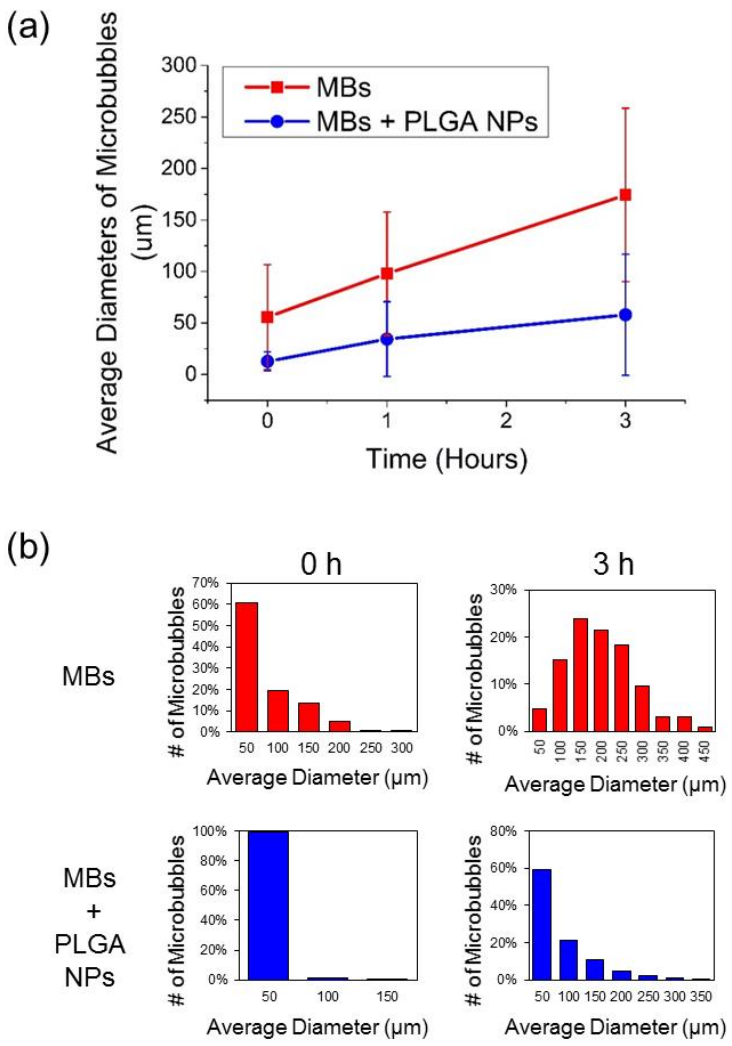

Figure 3.5. Size analysis of micorbubbles with and without PLGA nanoparticle coating. (a) The growth trend of microbubbles made of 1% w/w polymer solution at both conditions with and without PLGA nanoparticle coating, incubated at 37 °C for 3 hours. (b) The histogram of microbubbles at 0 hour and 3 hours with and without PLGA nanoparticles. (MBs: microbubbles; MBs + PLGA NPs: microbubbles coated with PLGA nanoparticles.)

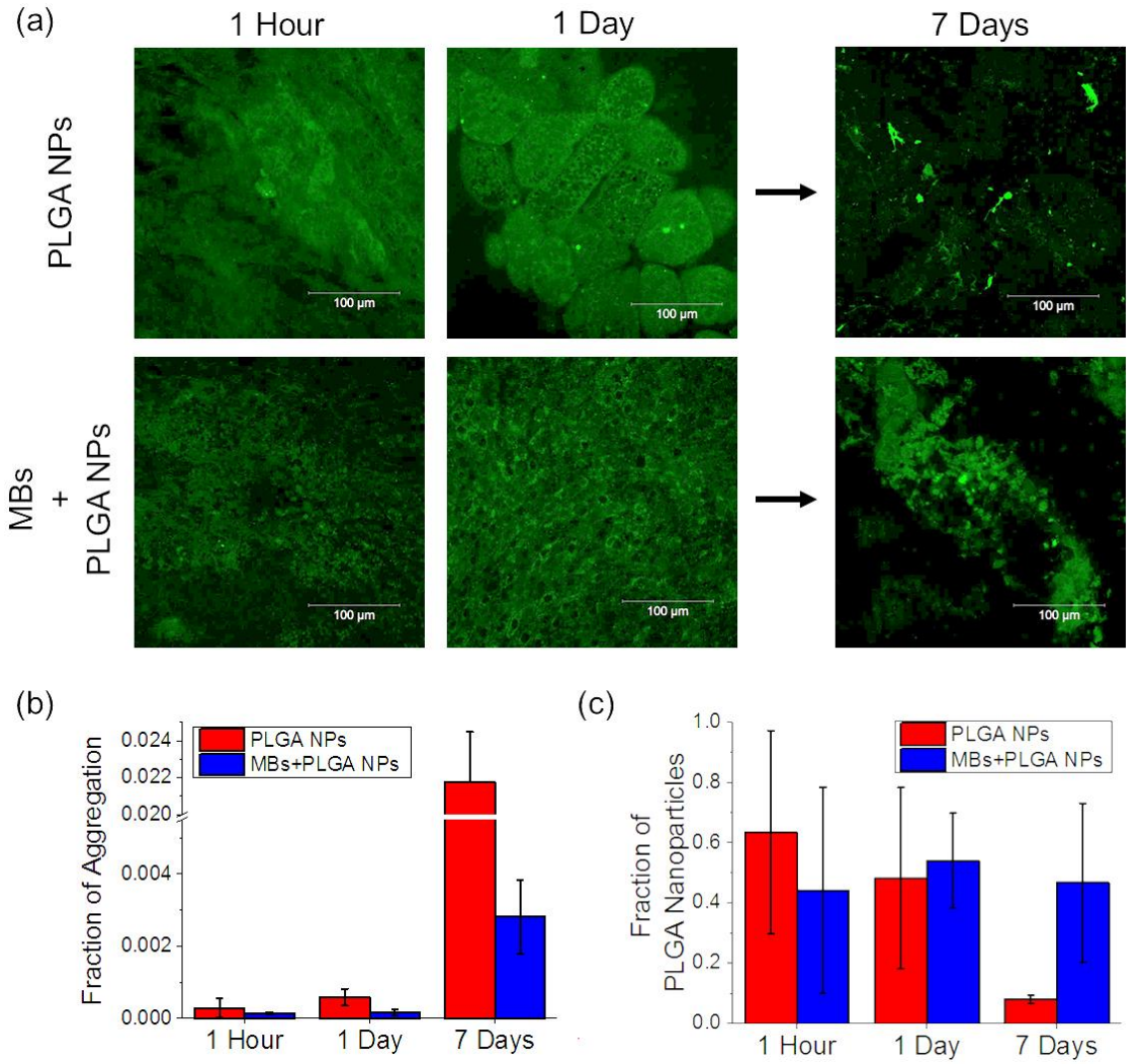

Figure 3.6. In vivo evaluation of PLGA nanoparticle retention. (a) The confocal microscopy images of CAMs incubated with FITC-labeled PLGA nanoparticles with and without microbubbles at different time points. (b) The quantified aggregation fraction for each condition. (c) The quantified fraction of remaining PLGA nanoparticles for each condition.

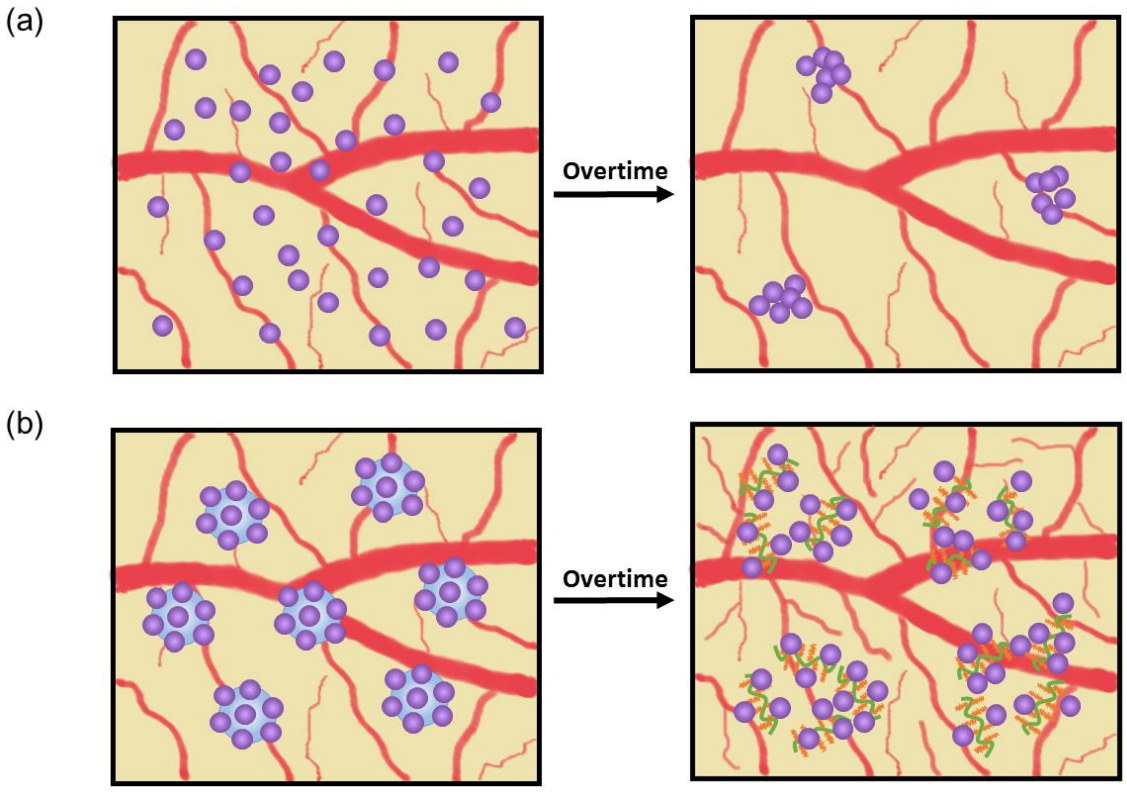

Figure 3.7. Proposed scheme of PLGA nanoparticles on CAMs with and without microbubbles. (a) PLGA nanoparticles without microbubbles replace and aggregate quickly overtime. (b) PLGA nanoparticles are localized by microbubbles and associated with polymer after bubble rapture.

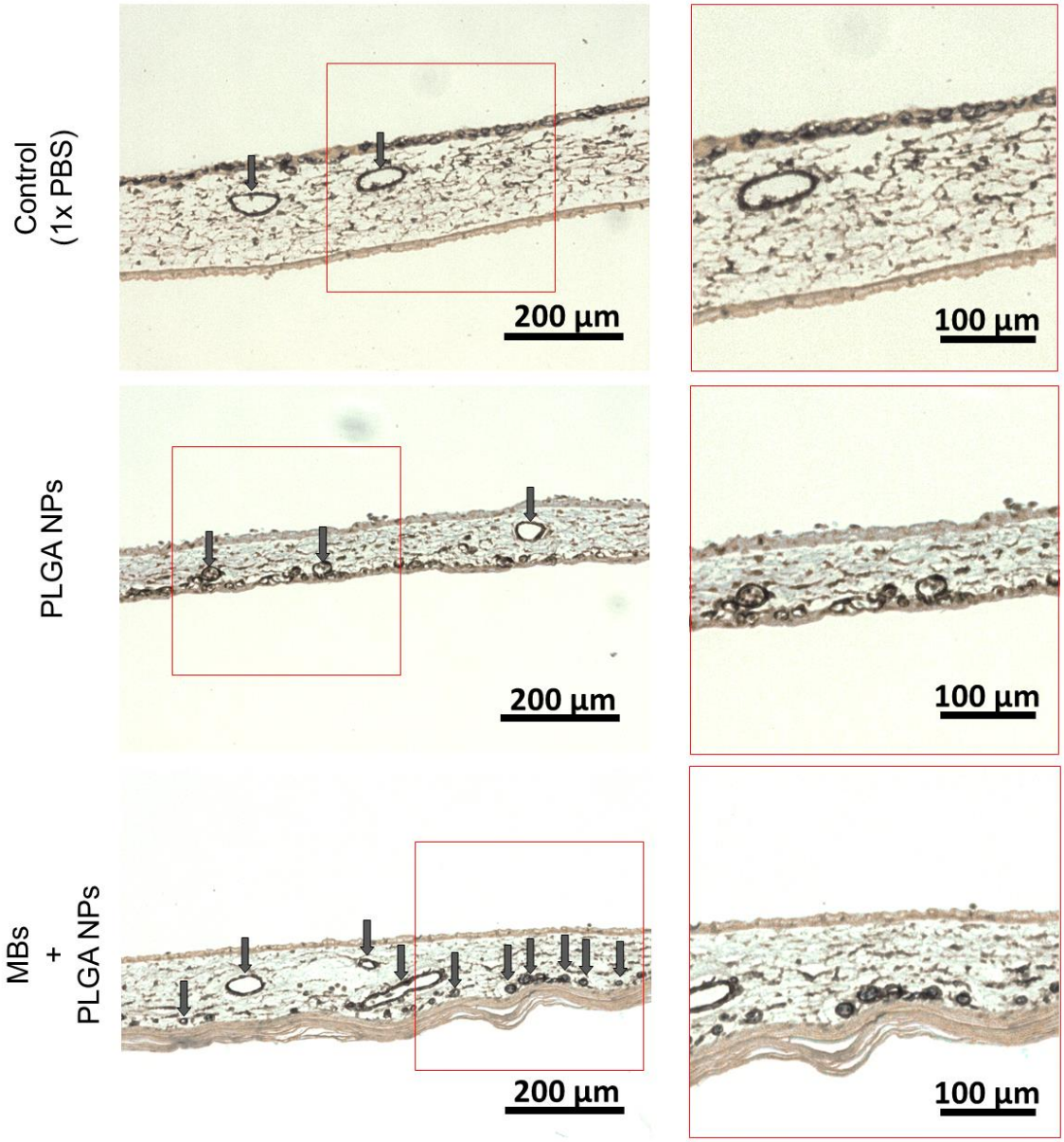

Figure 3.8. Histological images of CAM cross sessions at three different conditions. (PLGA-Ang1 NPs: Angiopoietin 1-loaded PLGA nanoparticles; MBs + PLGA-Ang1 NPs: microbubbles coated with Angiopoietin 1-loaded PLGA nanoparticles.)

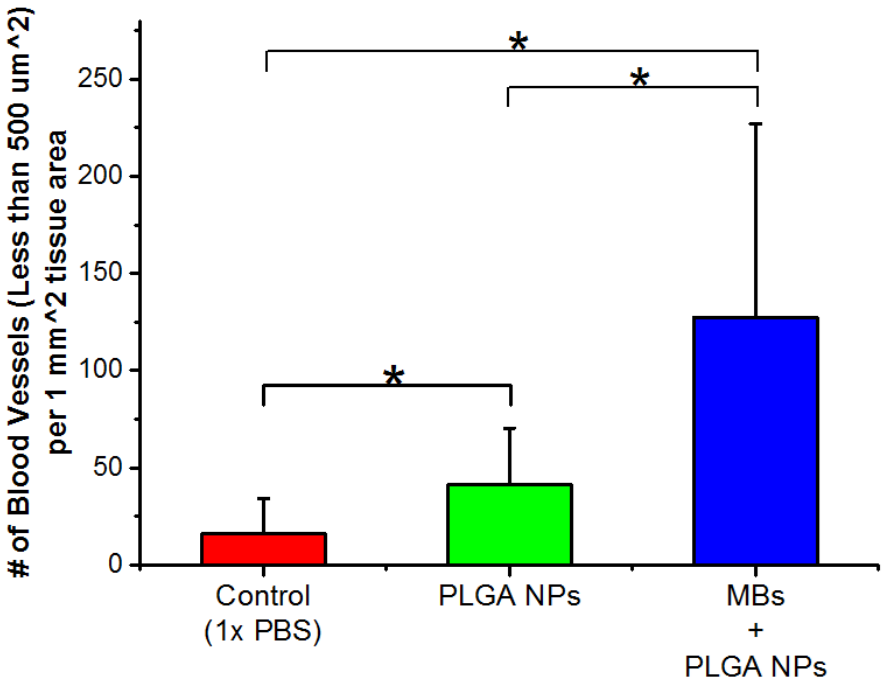

Figure 3.9. Quantified number of blood vessels with cross sectional area less than 500 μm^2 per 1 mm^2 tissue area. (*: statistical p value less than 0.05; 9 samples were measured for each condition.)

Table 3.1. Analysis of van der Waals potential for different particle interaction

	R_1 (µm)	R_2 (µm)	V_A (10^{-20} J)
Nanoparticle - Microbubble	0.05	5	-53.6
	0.05	50	-54.1
	0.05	100	-54.1
Nanoparticle - Nanoparticle	0.05	0.05	-27.1

Chapter 4

CONCLUSION

4.1 Summary

The study demonstrated the nanoparticle coating on microbubbles through van der Waals attraction by simply replacing the media without any further surface modification. The coating of nanoparticles on microbubble surface prolonged the microbubble life time by effectively reducing the direct interaction between microbubbles. Besides the coating, the size and stability of microbubbles was also related to the concentration of polymer solution; the initial size of microbubbles did not change much after certain point, but the stability was enhanced with high packing density of polymers. Along with the improved stability of microbubbles with nanoparticle coating, microbubbles helped to localize the nanoparticles with minimalized aggregation. With nanoparticles loaded with angiopoietin-1, the microbubbles helped to enhance the drug release performance over time at the desired sites. The CAM assay showed that drug-loaded nanoparticles co-existed with microbubbles initiated evenly distributed blood vessels, which was helpful on setting up new blood vessel network for nutrient transport.

4.2 Future Work

For future studies, it will be important further stabilize the microbubbles to reach the better result on localizing the drug-loaded nanoparticles. The stabilization of microbubbles can be done through modifying the polymer with polyethylene glycol,

which is widely used to prolong the life time of nanoparticles in physiological condition. Furthermore, to test the efficacy of the microbubble-nanoparticle system with vascularization drug on damaged tissue is important to confirm that evenly initiated blood vessel network works better in tissue repairing.

Furthermore, due to features of microbubbles, we suggest to apply this drug delivery system, microbubbles combined with drug-loaded nanoparticles, coupled with ultrasound imaging since microbubbles are well known as ultrasound contrast agents or ultrasound triggered microbubble rapture to direct the drug delivery. In this regard, the system can be develop for imaging-guided drug delivery.

REFERENCES

1. G. J. Nohynek, J. Lademann, C. Ribaud, M. S. Roberts, *Critical Reviews in Toxicology*, 2007, **37** (3), 251.

2. R. Peters, E. Kramer, A. G. Oomen, Z. E. Rivera, G. Oegema, P. C. Tromp, R. Fokkink, A. Rietved, H. J. Marvin, S. Weigel, A. A. Peijnenburg, H. Bouwmeester, *ACS Nano*, 2012, **6** (3), 2441.

3. C. Buzea, I. I. Pacheco, K. Robbie, *Biointerphases*, 2007, **2** (4), MR17.

4. V. V. Mody, R. Siwale, A. Singh, H. R. Mody, *Journal of Pharmacy and BioAllied Sciences*, 2010, **2** (4), 282.

5. R. Subbiah, M. Veerapandian, K. S. Yun, *Current Medicinal Chemistry*, 2010, **17**, 4559.

6. P. D. Howes, R. Chandrawati, M. M. Stevens, *Science*, 2014, **346** (6205), 53.

7. W. H. De Jong, P. J. A. Borm, *International Journal of Nanomedicine*, 2008, **3** (2), 133.

8. A. Z. Wilczewska, K. Niemirowicz, K. H. Markiewicz, H. Car, *Pharmacological Reports*, 2012, **64**, 1020.

9. S. Parveen, R. Misra, S. K. Sahoo, *Nanomedicine: Nanotechnology, Biology and Medicine*, 2012, **8** (2), 147.

10. A. Kumari, S. K. Yadav, S. C. Yadav, *Colloids and Surface B: Biointerfaces*, 2010, **75** (1), 1.

11. T. Sun, Y. S. Zhang, B. Pang, D. C. Hyun, M. Yang, Y. Xia, *Angewadte Chemie International Edition*, 2014, **53** (46), 12320.

12. S.-D. Li, L. Huang, *Molecular Pharmaceutics*, 2008, **5** (4), 496.

13. L. T. M. Sa, M. S. Albernaz, B. F. C. Patricio, M. V. F. Junior, B. F. Coelho, A. Bordim, J. C. Almeida, R. Santos-Oliveira, *Journal of Pharmaceutical and Biomedical Analysis*, 2012, **70**, 602.

14. R. Kumar, I. Roy, T. Y. Ohulchanskky, L. A. Vathy, E. J. Bergey, M. Sajjad, P. N. Prasad, *ACS Nano*, 2010, **4** (2), 699.

15. R. J. DeVolder, H. J. Kong, *Biomaterials*, 2010, **31**, 6494.

16. M. Morgen, D. Tung, B. Boras, W. Miller, A. M. Malfait, M. Tortorella, *Pharm. Res.*, 2013, **30**, 257.

17. M. Tomida, T. Nakato, S. Matsunami, T. Kakuchi, *Polymer*, 1997, **38** (18), 4733.

18. P. Caliceti, S. M. Quarta, F. M. Veronese, G. Cavallaro, E. Pedone, G. Giammona, *Biochimica et Biophysica Acta*, 2001, **1528**, 177.

19. R. Tadmor, *J. Phys.: Condens. Matter*, 2001, **13**, 195.

20. A. C. Pierre, *Introduction to Sol-Gel Processing*, Kluwer Academic Publishers, Massachusetts, 1st edn., 1998.

21. N. P. J. Brindle, P. Saharinen, K. Alitalo, *Circulation Research*, 2006, **98**, 1014.